

Machine Learning of Free Energies in Chemical Compound Space Using Ensemble Representations: Reaching Experimental Solvation Accuracy

Jan Weinreich

University of Vienna, Faculty of Physics, Kolingasse 14-16, AT-1090 Wien, Austria

Nicholas J. Browning

*Institute of Physical Chemistry and National Center for Computational Design and Discovery of Novel Materials (MARVEL),
Department of Chemistry, University of Basel, Klingelbergstrasse 80, CH-4056 Basel, Switzerland*

O. Anatole von Lilienfeld

*University of Vienna, Faculty of Physics, Kolingasse 14-16, AT-1090 Wien, Austria and
Institute of Physical Chemistry and National Center for Computational Design and Discovery of Novel Materials (MARVEL),
Department of Chemistry, University of Basel, Klingelbergstrasse 80, CH-4056 Basel, Switzerland*

(Dated: June 9, 2022)

Free energies govern the behavior of soft and liquid matter, and improved predictions could have a large impact on the development of drugs, electrolytes and homogeneous catalysts. Unfortunately, it is challenging to devise an accurate description of effects governing solvation such as hydrogen-bonding, van der Waals interactions, or entropy and conformational sampling. We present a machine learning approach for free energies based on a representation that employs computationally efficient Boltzmann averages for an approximated sampling of configurational space. Using the FreeSolv database, our out-of-sample prediction errors of experimental hydration free energies decay systematically with training set size, and experimental accuracy is reached after training on 80% (490 molecules). Corresponding model errors are on par or better than state-of-the art, physics based, legacy approaches. To generate the input representation of a new query compound, the model requires approximate and short molecular dynamics runs. We showcase the usefulness of this method through analysis of predicted solvation free energies for 116k organic molecules (all force-field compatible molecules in QM9 database) identifying the most and least solvated systems, and rediscovering quasi-linear structure property relationships in terms of hydrogen-bond donors, number of NH or OH groups, oxygen-content in hydrocarbons, and number of heavy atoms. We observe that the model’s accuracy is maximal when the temperature used for the molecular dynamics simulation to generate averaged input representation samples in training is the same as for the query compounds. Furthermore, the model’s error converges w.r.t. sampling time for both training and testing.

I. INTRODUCTION

An accurate description of solvation free energy is fundamentally important to rationalizing reaction kinetics and product propensities. Therefore accurate models describing solvation have far reaching utility from drug design to battery development. Computational methods for predicting solvation free energies based on *ab initio* methods^{1–4}, while accurate in principle, impose an extremely high computational burden and are therefore inherently limited when it comes to routine explorations of chemical compound space. Conversely, more readily available methods based on parametrized force-fields (FFs), implicit solvent models (PCM^{5,6}, GBSA⁷, SMD⁸, COSMO^{9,10}, COSMO-RS¹¹) or hybrid models (3D-RISM^{12–14}) trade improved computational expense for lower experimental accuracy. In particular, continuum solvation models exhibit several disadvantages including lack of locality in differentiating atomic environments^{15,16}, poor modeling of hydrogen bonding, inaccurate entropic contributions¹⁷ as well as poor decoupling between short-range and long-range effects.

The recent success of machine learning (ML) in the

domain of theoretical and computational chemistry is due to unprecedented availability of calculated single-point geometry quantum data has been manifested for challenging molecular problems, such accurate prediction of molecular properties¹⁸, atomization energies^{19?}, application to elpasolites²⁰, carbenes²¹, excited states²² or fragment based learning with AMONS²³. ML based free energy models, on the other hand, are much less established, and potential applications to explore chemical compound space in terms of thermodynamic properties have largely remained unexplored. Here, we propose to establish a new workflow for predicting ensemble properties, such as free energies of solvation ΔG_{sol} . In particular an adapted method for free energy ML is introduced with the ambition to provide both computational efficiency and high accuracy w.r.t. experiment. With this we address a missing concept of ML in material science by accounting for an ensemble of molecular conformations corresponding to different representations^{24–26} thus potentially leading to ambiguous predictions of ensemble properties.

We begin by detailing the ML workflow in sec. II with emphasis on the ensemble based representation. Next we present the results in sec. IV starting with a nu-

merical demonstration of the necessity of the ensemble representation before assessing the accuracy of free energy ML. Finally, we demonstrate the feasibility of the method for high throughput free energy predictions of 116k molecules revealing trends between molecular structure and solubility.

II. THEORY

We propose a representation based on an ensemble of conformers generated through MD sampling. This gives rise to a unique and temperature dependent representation of the system state.

Since this ML representation is rooted in statistical mechanics a physics based approach is introduced which distinguishes this work from other contributions to this topic^{27–30}. Furthermore a comparison with state-of-the art solvation models reveals that our ML approach retains the promise of being faster, more transferable and extendable than solvation methods based on conventional fitting of model parameters. While we focus on free energies of solvation we note that the same methodology might open new pathways for ML applications to protein binding or other ensemble properties like enthalpy and entropy.

We use kernel ridge regression²⁶ (KRR) a supervised ML method³¹ where the input is mapped to a high-dimensional feature space facilitating the regression problem. The similarity between molecules i, j with representations $\mathbf{X}_i, \mathbf{X}_j$ is measured by applying Gaussian kernel functions K ,

$$K(\mathbf{X}_i, \mathbf{X}_j) = \exp\left(-\frac{\|\mathbf{X}_i - \mathbf{X}_j\|_2^2}{2\sigma^2}\right), \quad (1)$$

where σ is the kernel width hyperparameter. The prediction of a property p_q of a query compound q is given by,

$$p(\mathbf{X}_q) = \sum_i^N \alpha_i K(\mathbf{X}_i^{\text{train.}}, \mathbf{X}_q), \quad (2)$$

where $K(\mathbf{X}_i^{\text{train.}}, \mathbf{X}_q)$ are kernel functions evaluated on the query and all training compounds with weight coefficients α . The unique solution vector for the optimal set of regression coefficients α is given by,

$$\alpha = (\mathbf{K} + \lambda \cdot \mathbf{1})^{-1} \mathbf{p}, \quad (3)$$

with the vector \mathbf{p} containing all values of the target property in the training set and regularization parameter λ . We emphasize that free energy is a property of an ensemble of possible states, while quantum machine learning (QML) is commonly used for quantum properties associated with exactly one given conformation of a molecule.

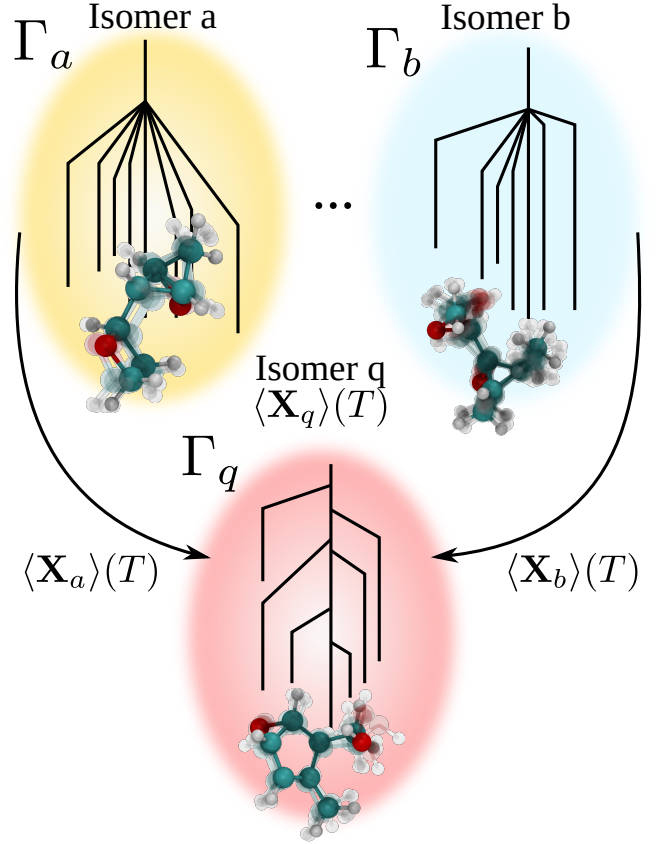


FIG. 1. The FML prediction for a new query compound q depends on the phase space $\{\Gamma_i\}$ of all training compounds consisting of conformers, depicted by disconnectivity graphs, sampled at the same temperature T , by virtue of ensemble average representations $\langle \mathbf{X} \rangle(T)$.

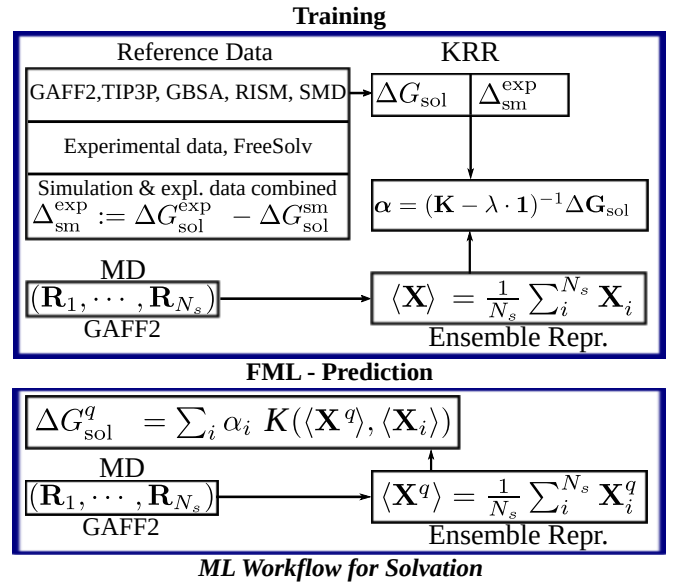


FIG. 2. Steps for training an FML model for the free energy of solvation ΔG_{sol} (upper box) and for prediction of ΔG_{sol}^q for a new query compound q (lower box).

Hence an intriguing question is how to design a physics based representation of a molecule for an ensemble property such as the free energy of solvation.

To this end we use FCHL19^{24,25} a many body representation that includes two and three-body terms where the first term accounts for interatomic distances and the second term for relative orientations of triplets of atoms. In this spirit, representations for thermodynamic properties should be designed similarly, taking into account the ensemble of accessible configurations at a given temperature. We use a thermodynamic ensemble average allowing for a unique definition of a representation given a set of conformers obtained by MD simulations at temperature T (s. sec. III). First the FCHL19 representation $\mathbf{X}(\{\mathbf{r}_i\})$ is computed for all conformers i before taking the ensemble average as follows,

$$\begin{aligned} \langle \mathbf{X} \rangle(T) &= \frac{1}{Z} \int_{\Gamma(T)} \mathbf{X}(\{\mathbf{r}_i\}) e^{-\beta E_i} d\Gamma \\ &\approx \frac{1}{N_s} \sum_i^{N_s} \mathbf{X}_i, \end{aligned} \quad (4)$$

with N_s uncorrelated gas-phase solute samples weighted by the respective Boltzmann factor $e^{-\beta E_i}$ with $\beta = \frac{1}{k_B T}$ and Z is the partition function. Note that the average representation $\langle \mathbf{X} \rangle(T)$ depends on T since both the integration domain $\Gamma(T)$ over phase space and the Boltzmann factors depend on T . This representation is similar to what was presented in³², however we use experimental free energies for training, because of the inherent accuracy deficiencies of implicit solvation models¹⁷.

We will refer to KRR using the vacuum geometry as QML and to free energy machine learning using the ensemble averaged FCHL19 representation as FML for the remainder of this paper. Note that unlike most applications of QML we train on experimental data and not on results from FP calculations and we emphasize that in our context QML has nothing to do with quantum computation. The methodology of FML is fully transferable to free energies from any level of theory and *ab initio* in the sense that solely molecular geometries are required. As illustrated in Fig. 1 the prediction of an ensemble property for a query compound q at temperature T depends on the phase spaces $\{\Gamma_i\}$ of all training molecules i . From this point of view FML infers predictions by combining information of all phase spaces by virtue of the average representation $\langle \mathbf{X} \rangle$ as an integral over conformer space. In Fig. 2 we show the practical steps for training a FML model for free energies of solvation, first a set of free energies is calculated or experimental values are collected from the literature. Subsequently and for all solute configurations the average over all representations of the trajectories is computed (s. Eq. 4), finally the regression weights α are determined (s. Eq. 3).

To illustrate the importance of an ensemble based approach we use QML to predict a hypothetical value of ΔG_{sol} for all possible fixed conformers of several stereo-

isomers. We emphasize that for an ML model to be consistent the predictions for free energies of solvation of a set of conformers should differ less than the experimental uncertainty. However, in the following we will show that QML based on a single molecular conformation can lead to inconsistent predictions. For training the QML model we use experimental free energies and representation vectors \mathbf{X}_{vac} based on vacuum geometries provided by the FreeSolv³³ database.

We randomly select four isomers of $\text{C}_7\text{H}_{10}\text{O}_2$ and use their complete set of conformers resulting from systematic scanning of all dihedral angles of the isomers³⁴ to compare the FML and QML predictions.

The distributions of the QML predictions reveal that for different conformers of the same isomer I_i , the predicted free energy ΔG_{sol} can vary by several kcal mol^{-1} (s. Fig. 3). Since hundreds of conformer minima may exist for one isomer, here $N(I_1), \dots, N(I_4) = 976, 661, 761, 13$, using a single geometry for the representation should clearly be avoided as it may lead to large prediction errors. Interestingly, we find (s. sec. IV)

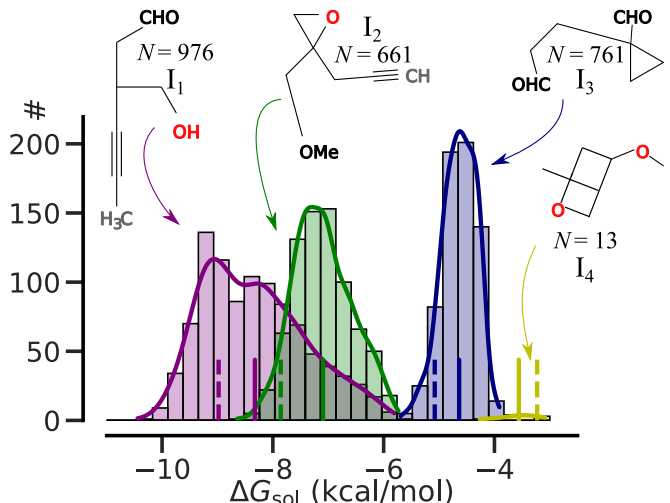


FIG. 3. Distribution of hydration free energies of conformers at 298K estimated by QML for four constitutional isomers ($\text{C}_7\text{H}_{10}\text{O}_2$). Corresponding FML estimates, as well as averages, are denoted by solid and dashed vertical lines, respectively. Insets show molecular graphs of corresponding constitutional isomers and number of conformers.

that due to an error cancellation QML based on vacuum geometries with weight coefficients α^{vac} can reach MAEs comparable with FML (s. sec. IV A). The reason is that the average of the QML predictions over a set of conformers, denoted by $\langle \cdot \rangle_c$ is close to the FML prediction,

$$\underbrace{\left\langle \sum_i^N \alpha_i^{\text{QML}} K(\mathbf{X}_i^{\text{QML}}, \mathbf{X}_c) \right\rangle_c}_{\text{Average QML}} \approx \underbrace{\sum_j^N \alpha_j^{\text{FML}} K(\langle \mathbf{X}_j \rangle, \langle \mathbf{X}_c \rangle_c)}_{\text{FML}}, \quad (5)$$

using the average representation over all conformers

$\langle \mathbf{X}_c \rangle_c$. This can be seen by inspecting Fig. 3, where the FML prediction of the average representation of all conformers is shown as a dashed line and the average of the individual conformer QML free energies as a solid line. The FML weight coefficients α^{FML} are obtained using the representation average $\langle \mathbf{X}_j \rangle$ (s. Eq. 4) over $N_s^{\text{train}} = 300$ MD samples (s. Fig. 2).

A. Δ -Machine Learning

Next we discuss the workflow for construction of FML models based on a combination of free energies obtained by solvation models (sm) with experimental (exp) data. Using Δ -ML³⁵ we promote solvation model free energies $\Delta G_{\text{sol}}^{\text{sm}}$ to experimental accuracy with the following correction terms,

$$\Delta_{\text{sm}}^{\text{exp}} = \Delta G_{\text{sol}}^{\text{exp}} - \Delta G_{\text{sol}}^{\text{sm}}. \quad (6)$$

Note that the FML correction is different for each compound accounting for too negative as well as too positive baseline free energies. The step for promoting free energies to a predicted experimental value $\Delta G_{\text{sol}}^{\text{exp}}(\text{FML})$ is given by,

$$\Delta G_{\text{sol}}^{\text{exp}}(\text{FML}) = \Delta G_{\text{sol}}^{\text{sm}} + \Delta_{\text{sm}}^{\text{exp}}. \quad (7)$$

Besides these modifications the workflow remains the same as in Fig. 2.

III. COMPUTATIONAL DETAILS

A. Molecular Dynamics

All MD simulations are performed with OpenMM³⁶ in vacuum and the NVT ensemble using a Langevin integrator with a friction coefficient of 1 ps^{-1} and the small molecule FF GAFF2^{37,38} with a time-step of $\Delta t = 2 \text{ fs}$ and total simulation time of 2 ns using SHAKE³⁹. Partial charges are computed with antechamber^{37,38} at AM1-BCC⁴⁰ level. An exception are the implicit solvent GBSA^{41,42} simulations where we use AMBER³⁷/GAFF³⁸ while all other simulation parameters are the same. MD samples were selected with 2 ps separation which is well beyond the correlation time of $\sim 0.5 \text{ ps}$.

B. Machine Learning

To optimize the hyper-parameters σ and λ (s. Eqns. 1, 3), we perform 10-fold cross validation on the training set only and validate the performance on the test set using the QML package⁴³. The training set contains all FreeSolv³³ molecules except for 146 test set

molecules which overlap with the QM9 database. Histograms showing the free energy distribution and the size of all molecules in the FreeSolv database are shown in the SI. For numerous FreeSolv compounds no value for the experimental error is reported, but a default value of $0.6 \text{ kcal mol}^{-1}$ corresponding to thermal energy fluctuations at 298.15 K is assumed which we use as our target accuracy, albeit the total average absolute error of all experimental values is slightly smaller ($0.55 \text{ kcal mol}^{-1}$).

IV. RESULTS

A. Learning Curves and Free Energies of 116k Molecules

Next we discuss the performance of several ML models by studying learning curves i.e. the MAE as a function of training set size N (s. Fig. 4). Most notably we assess FML and the ensemble average representation (s. Eq. 4) and Δ -ML (s. Eq. 7) for predicting experimental free energies of the FreeSolv³³ database.

In addition we also test the RDKit⁴⁴ implementation of the extended connectivity fingerprint⁴⁵ (ECFP4) commonly used in cheminformatics and secondly a custom QSAR based representation, named CQ (s. SI). To compare KRR with conventional fitting methods we also report the MAEs of a multilinear regression model with CQ. The error bars and colored areas in Fig. 4 show the standard deviation of the MAEs resulting from 10-fold cross validation over the FreeSolv database. We find that feature based models ECFP4 and CQ (s. Fig. 4a) perform worst reaching a MAE of $0.8 \text{ kcal mol}^{-1}$ for a maximal training set size of $N_{\text{max}} = 550$. This could be expected, because feature based representations cannot distinguish between molecular conformations which can have a large influence on predictions of ΔG_{sol} (s. sec. II).

QML on the other hand hits the target accuracy, the experimental accuracy of $0.6 \text{ kcal mol}^{-1}$ for about $N_{\text{max}} = 550$ training molecules. The best FML model trained with 10 random MD samples per molecule with $T = 350 \text{ K}$ essentially results in the same MAE. While both models reach the experimental accuracy, we find that FML has a slightly smaller offset hitting 1 kcal mol^{-1} for $N \approx 50$ while the QML model trained on the vacuum geometries has a MAE of about $1.5 \text{ kcal mol}^{-1}$. The otherwise similar performance of both models may to some extent be attributed to the error compensation we discussed in Eq. 5.

Next we focus on Δ -ML³⁵ using various solvation models as a baseline such as GBSA (GAFF^{37,38}), 3D-RISM^{12,13} (GAFF^{37,38}/TIP3P⁴⁶) and SMD⁸ (M06-2X⁴⁷/Def2-TZVPP⁴⁸) and TI (GAFF2^{37,38}/TIP3P⁴⁶). The GBSA values have been computed using AMBER^{37,38} (s. sec. III), the TI values are from the FreeSolv³³ database and the values for the two implicit solvation methods 3D-RISM^{12,13} and SMD⁸ are

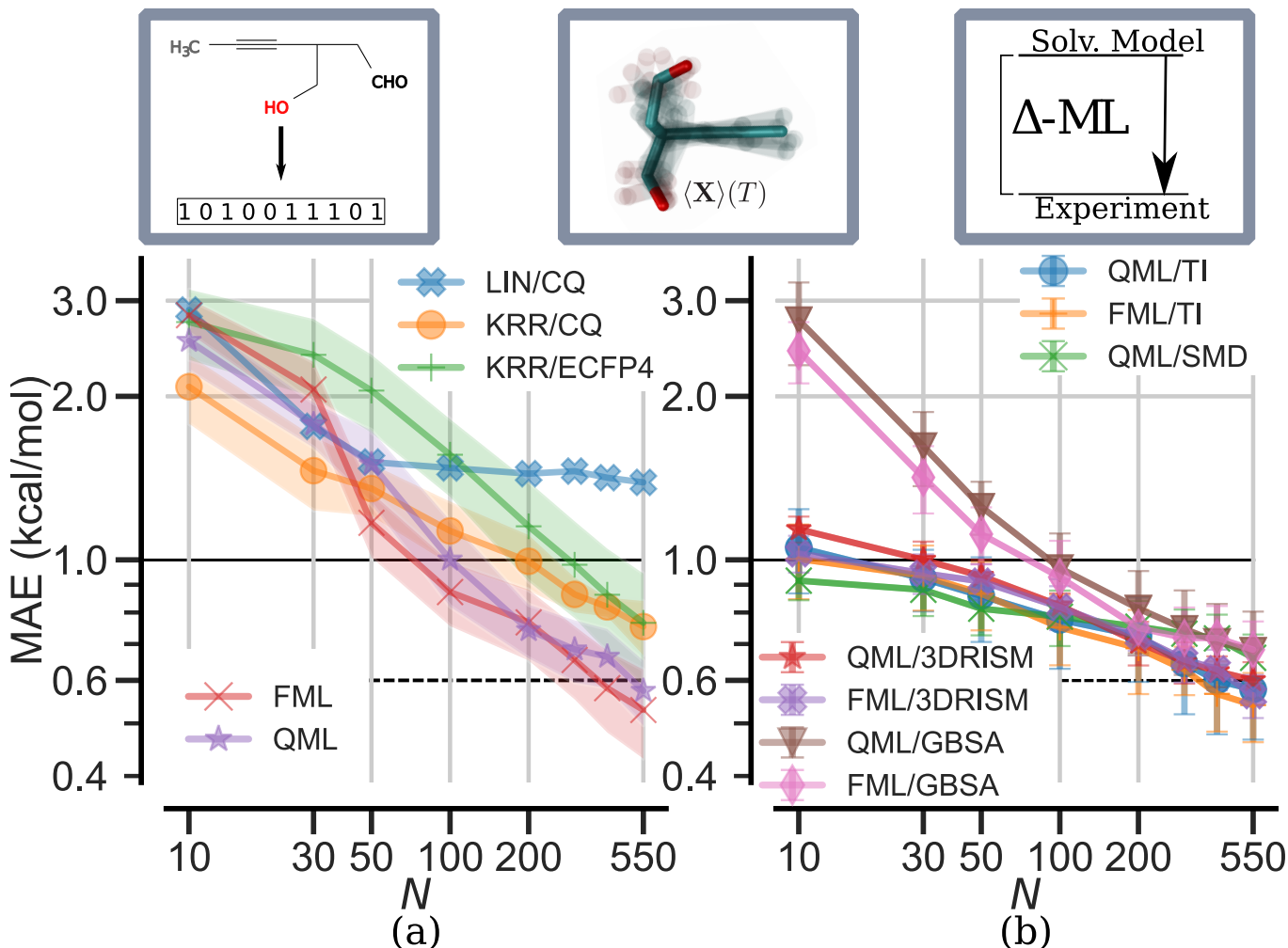


FIG. 4. Learning curves for free energies of FreeSolv database³³ including standard deviation at each number of training molecules N obtained by 10-fold cross-validation for feature based KRR, QML and FML in (a). QML/FML based Δ -ML with various solvation models as baseline in (b). Solid black line marks thermo-chemical accuracy at 1 kcal mol⁻¹, dashed line the experimental uncertainty (298 K $\cdot k_B \approx 0.6$ kcal mol⁻¹).

from the SI of¹⁴. We find that Δ -ML can lower the offset of the learning curves and thus may be useful if experimental data is rare. FML requires about 100 training molecules to reach 0.8 kcal mol⁻¹ whereas Δ -ML using TI or 3D-RISM only needs around 50. Note that the SMD baseline model has the lowest offset, since SMD has the smallest MAE of 0.93 kcal mol⁻¹ versus a MAE of 1.12 kcal mol⁻¹ for TI on the FreeSolv database. However, after around 150 compounds both approaches, direct FML and Δ -ML, perform similarly and converge to the target accuracy.

Similar observations were also reported in²⁸, but we find that the target accuracy can be reached using FML without additional solvation calculations for Δ -ML. We note that some caution is required for this comparison since the accuracy of Δ -ML relies heavily on systematic correlation between the baseline method and experimental data and thus potentially on the selected chemical

space.

To facilitate a comparison of various different solvation models and FML we show a scatter plot (s. Fig. 5) of FML predictions versus experiment. The training set consists of all molecules in FreeSolv but not in QM9, the overlap (146 molecules) is used as a test set. The MAEs for FML and the tested solvation models are listed in Tab. I. We find that the best FML model with $N_s^{\text{train}} = 10$ and $T_{\text{train}} = 350$ K results in a MAE of 0.57 kcal mol⁻¹ reaching the experimental accuracy of solvation energy measurements and performing slightly better than SMD with 0.61 kcal mol⁻¹. Note that FML has some significant outliers such as methane with an error of about 2 kcal mol⁻¹. The largest outlier however is 2-hydroxybenzaldehyde with an error of 3.6 kcal mol⁻¹. It is worth emphasizing that SMD uses at least 79 of the test set molecules for parameterization which were not included in training of the FML model. Still FML has a slightly smaller MAE despite using fewer train-

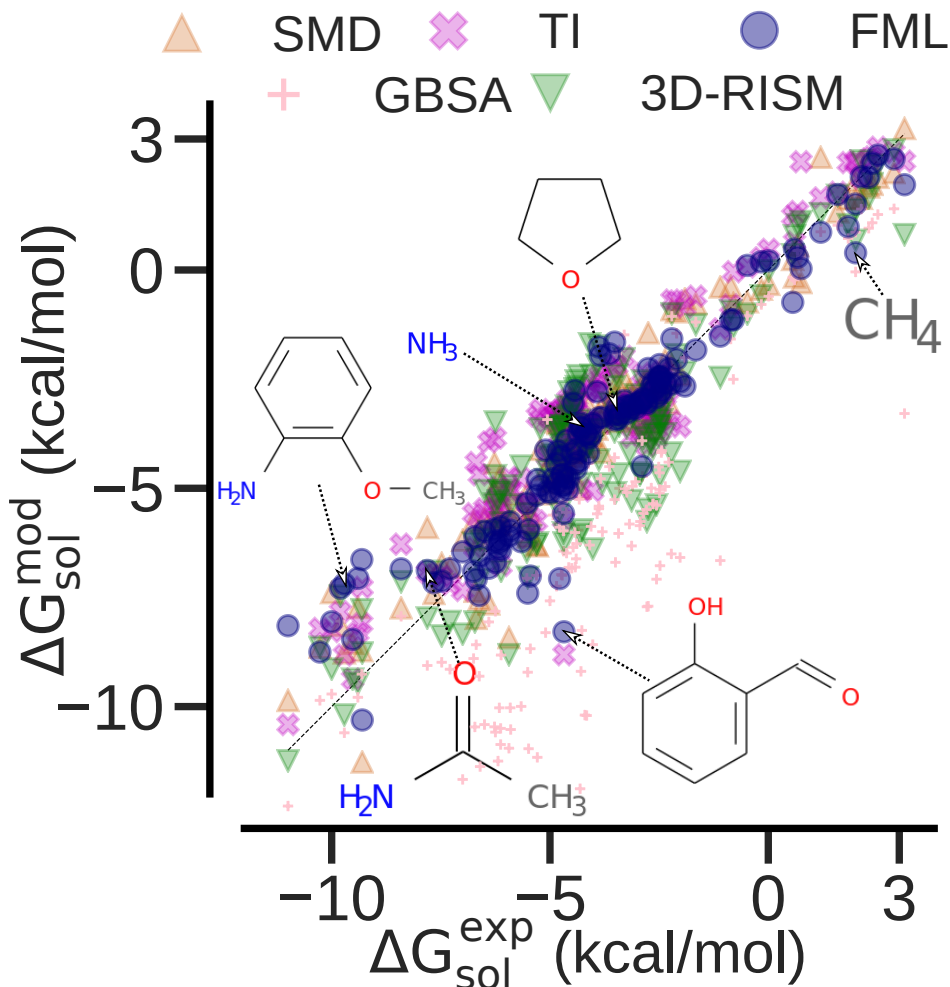


FIG. 5. Scatter plot comparing free energies of solvation predicted by FML(350 K; 10) (blue) using an ensemble based representation and solvation models: SMD (chocolate), TI (violet), 3D-RISM (green) and GBSA (pink). The FML predictions are also listed in the SI.

ing points compared to SMD. Furthermore we find that FML clearly outperforms TI and 3D-RISM reaching a MAE of 1 kcal mol^{-1} after about $N = 100$ training molecules. We emphasize that a typical SMD (M06-2X⁴⁷/Def2-TZVPP⁴⁸) calculation of a molecule in the FreeSolv database with Gaussian09⁴⁹ is *very* expensive while only a FF MD simulation in vacuum is required to sample a trajectory for the average representation and can be run on a single CPU in less than 10 minutes (s. Tab. I for timing benchmarks).

In addition FML clearly outperforms COSMO^{9,10,50} with B-P86^{51,52}/TZVP⁵³ resulting in a MAE of $1.94 \text{ kcal mol}^{-1}$ with higher computational costs. For comparison with COSMO-RS as implemented in COSMOtherm⁵⁴ we refer to a benchmark test^{11,55} with a set of 274 molecules resulting in a MAE of $0.52 \text{ kcal mol}^{-1}$ reaching the accuracy of FML but at higher computational cost (s. Tab. I) and as for all other DFT methods with a worse scaling with the number of atoms compared to FFs.

Finally we explore free energies of a large dataset of

molecules to identify trends between solubility and structure throughout chemical space. For this purpose we use 116k molecules of the QM9 dataset and study the predicted free energy distribution (s. Fig. 6a). As a comparison we also show the corresponding distribution of ΔG_{sol} for the FreeSolv database in the SI. The FML model was trained on the complete FreeSolv database with coincident QM9 molecules removed from training. We find that the free energy distribution is approximately Gaussian with a mean value of $\bar{\Delta G}_{\text{sol}} = -7.56 \text{ kcal mol}^{-1}$ spanning a range of $25.1 \text{ kcal mol}^{-1}$. The molecules with the most negative and positive ΔG_{sol} are QM9 compound with index 26712 with $-21.63 \text{ kcal mol}^{-1}$ and QM9 molecule with index 118570 with $3.47 \text{ kcal mol}^{-1}$ respectively (s. Fig. 6b,c). The top 50 most soluble and least soluble molecules according to FML are also shown in the SI. We find that the most soluble molecules have a planar ring structure. On the other hand the 4907 hydrocarbons of QM9 occupy the right tail of the distribution. Molecules with many hetero atoms bonded in NH/OH groups in a planar ring structure tend to have a very

TABLE I. Comparison of MAEs, Pearson’s r , estimated order of CPU time per solute prediction for various solvation models and FML. Approximate number of training molecules \tilde{N} needed for FML to reach the MAE of each respective method. The conversion factor from GPU to CPU $c = \frac{t_{\text{CPU}}}{t_{\text{GPU}}}$ may vary substantially between $\sim 10 - 60$ depending on hardware/MD code (here OpenMM³⁶). N_g is the number of grid points for TI, typically ~ 10 .

Class	Model	MAE (kcal/mol)	r	\tilde{N}	\sim cpu-h/solute	Reference	Year of Publication
DFT	SMD	0.61 ¹⁴	0.96	400	<i>high</i>	[8,49]	2009
	COSMO	1.94	0.90	20	10^{-1}	[9,10,50]	1993
	COSMO-RS	0.52 ⁵⁶	0.91	–	10^{-1}	[11,50,54,56]	2000
	DCOSMO-RS	0.94 ⁵⁶	0.87	100	10^{-1}	[57]	2006
FF	3D-RISM	0.99 ¹⁴	0.90	100	10^{-1}	[12,13]	1998
	TI	0.93 ³³	0.94	100	$N_g \times c \times 10^{-1}$	[33]	2017
	GBSA	2.41	0.84	20	10^{-2}	[41,42]	2004
ML	FML	0.57	0.95	490	10^{-2}	this work	2020

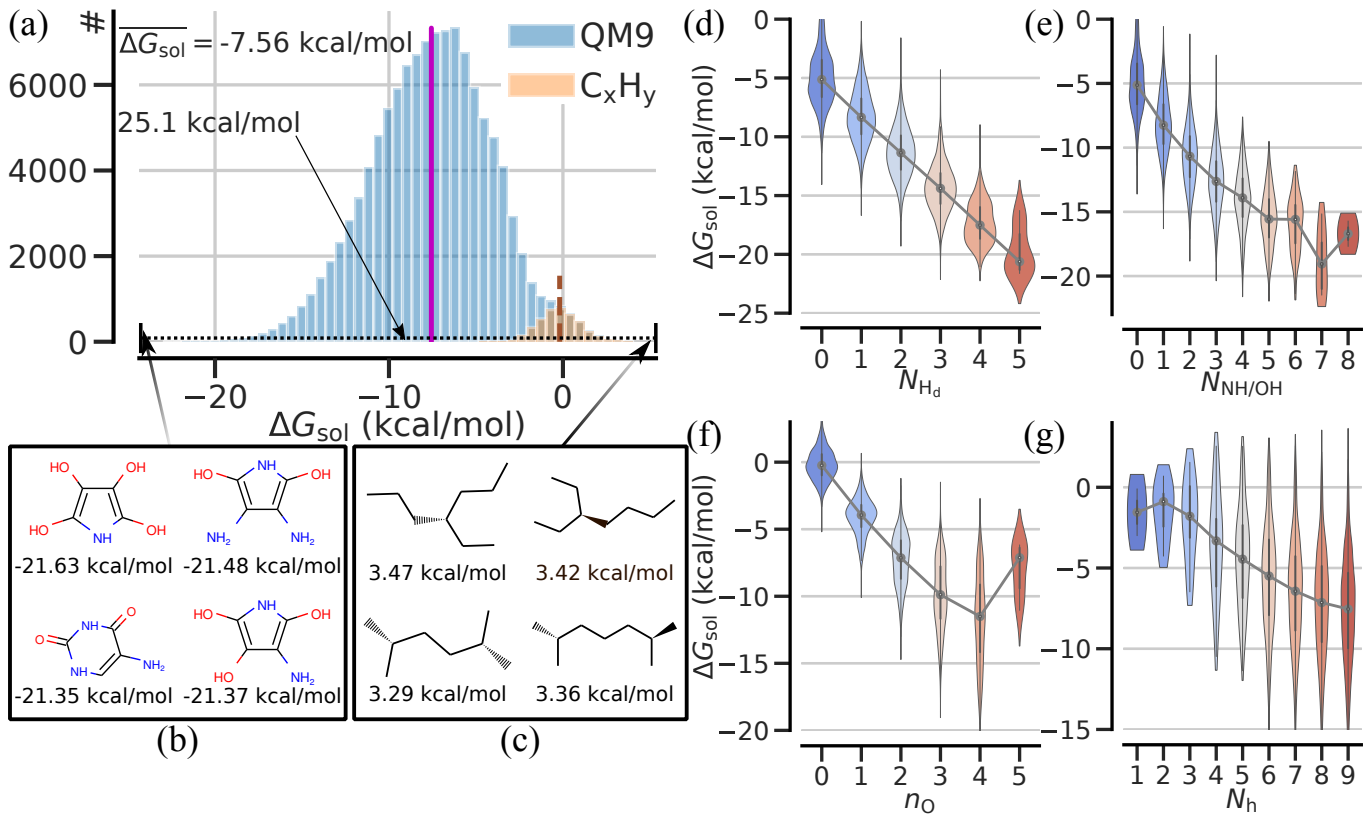


FIG. 6. Free energy distribution of 116k molecules predicted by FML in (a), small histogram corresponds to a sub set of 4907 hydrocarbons with averages shown as solid and dashed line respectively. Below, four molecules with most negative (b) and positive (c) ΔG_{sol} in clockwise order. The mean of ΔG_{sol} for structural features such as number of H-bond donors N_{Hd} (d) NH/OH groups $N_{\text{NH/OH}}$ (e) or oxygen atoms in stoichiometry $C_{n_C}H_{n_H}O_{n_O}$ (f) heavy atoms N_h (g).

negative ΔG_{sol} while aliphatic linear molecules tend to be less soluble. This can be explained by the large difference in electronegativity between the H and the N, O atoms leading to polar bonds eventually resulting in H-bonds, lowering the enthalpy of solvation. Alkanes on the other hand have a negligible polarity, and thus only interact with water through much weaker van der Waals interaction resulting in low solubility.

These simple rules for the solubility lead to trends for

the average free energy $\overline{\Delta G_{\text{sol}}}$ such as approximately linear relations with the number of H-bond donors N_{Hd} or the number of OH and NH groups $N_{\text{NH/OH}}$ as shown in Fig. 6de. Furthermore $\overline{\Delta G_{\text{sol}}}$ decreases with the number of oxygen atoms for molecules with stoichiometry $C_{n_C}H_{n_H}O_{n_O}$ and with the number of heavy atoms N_h (s. Fig. 6fg). The former effect is due to enthalpic H-bond contributions from hydroxyl groups and the latter

is due to weak van der Waals interactions which roughly scale with the molecule size. Such linear free-energy relationships (LFER) are well known and used for predictive models e.g. for solvation^{58,59} or organic chemistry⁶⁰.

B. Analysis of the Model

Having defined an ensemble average representation $\langle \mathbf{X} \rangle(T)$ (s. Eq. 4) we study the convergence of mean absolute errors (MAEs) as a function of the number of MD samples for the training N_s^{train} and test molecules N_s^{test} , where $T_{\text{test}} = T_{\text{train}} = 350$ K. By inspection of Fig. 7a we find that FML models trained with large N_s^{train} tend to have a larger offset in the MAEs and a larger number of test samples N_s^{test} is needed to reach the same accuracy as a model with small N_s^{train} . An extreme case

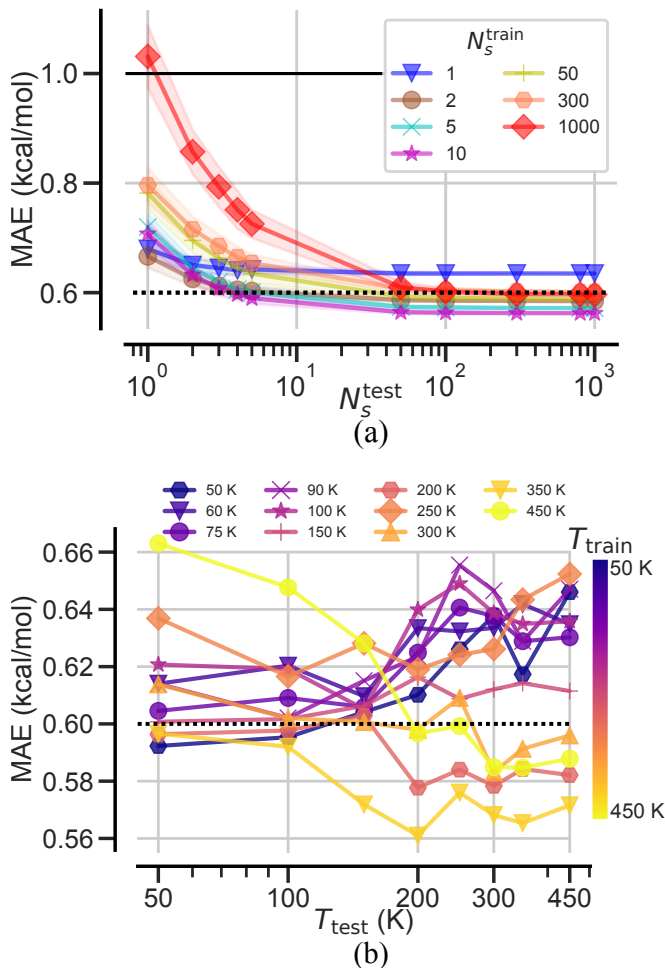


FIG. 7. Comparison of MAEs of FML models with average representations using different number of samples in the training and test molecule representation ($T_{\text{test}} = T_{\text{train}} = 350$ K) (a). Various temperatures for sampling the test T_{test} and training molecules T_{train} in (b) and resulting MAEs. Solid line marks thermo-chemical accuracy at 1 kcal mol^{-1} , dashed line the experimental uncertainty ($298 \text{ K} \cdot k_B \approx 0.6 \text{ kcal mol}^{-1}$).

is the model FML(350 K; 1) with only one MD sample with no improvement beyond $N_s^{\text{test}} \approx 10$ samples per test molecule, while all other ML models keep improving until the MAEs saturate at $N_s^{\text{test}} \approx 100$. Interestingly, we find that the accuracy increases only up to $N_s^{\text{train}} \approx 10$ and becomes worse beyond. While this seems counterintuitive it can be explained by the fact that FML models with 1000 samples for the average representation are biased to fully converged representations, thus more sensitive to noise in the data. Here addition of more samples can have the same effect as including a very distinct set of molecules for training which may also lead to worse predictions. Next we investigate the temperature dependence of the ensemble average representation. To this end the MAEs of several ML models FML(T_{train} ; N_s^{train}) with training molecule sampling temperatures T_{train} between 50 K and 450 K are compared for various test molecule sampling temperatures T_{test} with $N_s^{\text{train}} = N_s^{\text{test}} = 10$ (s. Fig. 7b). We find that FML models usually perform best if $T_{\text{train}} \approx T_{\text{test}}$, e.g. model FML(50 K) performs best for $T_{\text{train}} = T_{\text{test}} = 50$ K and the MAE increases for higher temperatures T_{test} . On the other hand, FML(450 K) performs much worse at low temperature than at high temperature. This indicates, as suggested by Eq. 4, that the average representation indeed results in models specific for the temperature and phase space $\Gamma(T)$ spanned by the training MD samples.

V. CONCLUSION

We demonstrated that ML for prediction of molecular ensemble properties should be rooted in statistical mechanics, since ML based on a single molecular geometry can lead to large prediction errors as discussed in Fig. 3. The definition of a representation based on Boltzmann weighted averages does not only resolve this issue but also introduces a temperature dependence.

In the same manner models could be constructed that depend on pressure or chemical potentials to account for increasingly more realistic ambient conditions. The assessment of FML is very encouraging, while not only performing as accurate or better than state of the art solvation models, experimental accuracy is achieved with unprecedented low computational cost. In addition we find that Δ -ML can improve the predictions for small training set sizes, however FML can reach experimental accuracy without requiring additional solvation model calculations.

Furthermore we emphasize that it is trivial to improve the accuracy and transferability of FML by adding more experimental data points while this is not necessarily true for other solvation models. Finally FML was applied to 116k organic molecules of the QM9 database (see Fig. 6) revealing that molecules with a high solubility tend to have many hetero atoms and are arranged in planar ring structures while linear aliphatic molecules tend to have a lower solubility. We could therefore demonstrate that

FML can be used to study the CCS of solvation and to find non-trivial structure-property relationships.

ACKNOWLEDGEMENT

O.A.v.L. acknowledges support from the Swiss National Science foundation (407540_167186 NFP 75 Big Data) and from the European Research Council (ERC-

CoG grant QML and H2020 projects BIG-MAP and TREX). This project has received funding from the European Union’s Horizon 2020 research and innovation programme under Grant Agreements #952165 and #957189. This result only reflects the author’s view and the EU is not responsible for any use that may be made of the information it contains. This work was partly supported by the NCCR MARVEL, funded by the Swiss National Science Foundation.

- ¹ R. Jinnouchi, F. Karsai, and G. Kresse, *Phys. Rev. B* **101**, 060201 (2020).
- ² Y. Basdogan, M. C. Groenenboom, E. Henderson, S. De, S. B. Rempe, and J. A. Keith, *J. Chem. Th. Comp.* **16**, 633 (2020).
- ³ L. Mones, A. Jones, A. W. Götz, T. Laino, R. C. Walker, B. Leimkuhler, G. Csányi, and N. Bernstein, *J. Comp. Chem.* **36**, 633 (2015).
- ⁴ H. Takahashi, H. Kambe, and A. Morita, *J. Chem. Phys.* **150**, 114109 (2019).
- ⁵ F. Fogolari, A. Brigo, and H. Molinari, *J. Mol. Recogn.* **15**, 377 (2002).
- ⁶ B. Mennucci, J. Tomasi, R. Cammi, and J. R. Cheeseman, *J. Phys. Chem. A* **106**, 6102 (2002).
- ⁷ A. V. Marenich, C. J. Cramer, and D. G. Truhlar, *J. Chem. Th. Comp.* **9**, 609 (2013).
- ⁸ A. V. Marenich, C. J. Cramer, and D. G. Truhlar, *J. Phys. Chem. B* **113**, 6378 (2009).
- ⁹ A. Klamt and G. Schüürmann, *J. Chem. Soc., Perkin Trans. 2*, 799 (1993).
- ¹⁰ A. Klamt, *J. Phys. Chem.* **99**, 2224 (1995).
- ¹¹ A. Klamt and F. Eckert, *Fluid Phase Equilibria* **172**, 43 (2000).
- ¹² D. Beglov and B. Roux, *J. Phys. Chem. B* **101**, 7821 (1997).
- ¹³ A. Kovalenko and F. Hirata, *Chem. Phys. Lett.* **290**, 237 (1998).
- ¹⁴ D. Roy and A. Kovalenko, *J. Phys. Chem. A* **123**, 4087 (2019).
- ¹⁵ Y. Basdogan, A. M. Maldonado, and J. A. Keith, *WIREs Comp. Mol. Sci.* **10**, e1446 (2020).
- ¹⁶ J. J. Guerard and J. S. Arey, *J. Chem. Th. Comp.* **9**, 5046 (2013).
- ¹⁷ J. Zhang, H. Zhang, T. Wu, Q. Wang, and D. van der Spoel, *J. Chem. Th. Comp.* **13**, 1034 (2017).
- ¹⁸ F. A. Faber, L. Hutchison, B. Huang, J. Gilmer, S. S. Schoenholz, G. E. Dahl, O. Vinyals, S. Kearnes, P. F. Riley, and O. A. von Lilienfeld, *J. Chem. Th. Comp.* **13**, 5255 (2017).
- ¹⁹ K. Hansen, G. Montavon, F. Biegler, S. Fazli, M. Rupp, M. Scheffler, O. A. von Lilienfeld, A. Tkatchenko, and K.-R. Müller, *J. Chem. Th. Comp.* **9**, 3404 (2013).
- ²⁰ F. A. Faber, A. Lindmaa, O. A. von Lilienfeld, and R. Armiento, *Phys. Rev. Lett.* **117**, 135502 (2016).
- ²¹ M. Schwilk, D. N. Tahchieva, and O. A. von Lilienfeld, “Large yet bounded: Spin gap ranges in carbenes,” (2020), [arXiv:2004.10600 \[physics.chem-ph\]](#).
- ²² J. Westermayr and P. Marquetand, “Machine learning for electronically excited states of molecules,” (2020), [arXiv:2007.05320 \[physics.chem-ph\]](#).
- ²³ B. Huang and A. von Lilienfeld, *Nature Chem.*, **1** (2020).
- ²⁴ A. S. Christensen, L. A. Bratholm, F. A. Faber, and O. A. von Lilienfeld, *J. Chem. Phys.* **152**, 044107 (2020).
- ²⁵ F. A. Faber, A. S. Christensen, B. Huang, and O. A. von Lilienfeld, *J. Chem. Phys.* **148**, 241717 (2018).
- ²⁶ B. Huang, N. O. Symonds, and O. A. von Lilienfeld, (2018), [arXiv:1807.04259](#).
- ²⁷ J. Gebhardt, M. Kiesel, S. Riniker, and N. Hansen, *J. Chem. Inf. Mod.* (2020), 10.1021/acs.jcim.0c00479, article ASAP.
- ²⁸ J. Scheen, W. Wu, A. S. J. S. Mey, P. Tosco, M. Mackey, and J. Michel, *J. Chem. Inf. Mod.* (2020), 10.1021/acs.jcim.0c00600, article ASAP.
- ²⁹ H. Lim and Y. Jung, “Mlsolv-a: A novel machine learning-based prediction of solvation free energies from pairwise atomistic interactions,” (2020), [arXiv:2005.06182 \[stat.ML\]](#).
- ³⁰ S. Axelrod and R. Gomez-Bombarelli, “Molecular machine learning with conformer ensembles,” (2020), [arXiv:2012.08452 \[cs.LG\]](#).
- ³¹ V. N. Vapnik, *Statistical Learning Theory* (Wiley-Interscience, 1998).
- ³² C. Rauer and T. Bereau, *J. Chem. Phys.* **153**, 014101 (2020).
- ³³ G. Duarte Ramos Matos, D. Y. Kyu, H. H. Loeffler, J. D. Chodera, M. R. Shirts, and D. L. Mobley, *J. Chem. Engin. Data* **62**, 1559 (2017).
- ³⁴ D. Lemm, J. C. Kromann, G. F. von Rudorff, and O. A. von Lilienfeld, To be submitted.
- ³⁵ R. Ramakrishnan, P. O. Dral, M. Rupp, and O. A. von Lilienfeld, *J. Chem. Th. Comp.* **11**, 2087 (2015).
- ³⁶ P. Eastman, J. Swails, J. D. Chodera, R. T. McGibbon, Y. Zhao, K. A. Beauchamp, L.-P. Wang, A. C. Simmonett, M. P. Harrigan, C. D. Stern, R. P. Wiewiora, B. R. Brooks, and V. S. Pande, *PLOS comp. bio.* **13**, e1005659 (2017).
- ³⁷ J. Wang, W. Wang, P. A. Kollman, and D. A. Case, *J. Mol. Graph. Model.* **25**, 247 (2006).
- ³⁸ J. Wang, R. M. Wolf, J. W. Caldwell, and P. A. Kollman, *J. Comp. Chem.* **25**, 1157 (2004).
- ³⁹ J.-P. Ryckaert, G. Ciccotti, and H. J. Berendsen, *J. Comp. Phys.* **23**, 327 (1977).
- ⁴⁰ A. Jakalian, B. Bush, D. Jack, and C. Bayly, *J. Comp. Chem.* **21**, 132 (2000).
- ⁴¹ A. Onufriev, D. Bashford, and D. A. Case, *Proteins* **55**, 383 (2004).
- ⁴² J. Weiser, P. S. Shenkin, and W. C. Still, *J. Comp. Chem.* **20**, 217 (1999).

- ⁴³ A. Christensen, F. Faber, B. Huang, L. Bratholm, A. Tkatchenko, K. Müller, and O. v. Lilienfeld, To be submitted (2017), <https://github.com/qmlcode/qml>.
- ⁴⁴ “Rdkit: Open-source cheminformatics,” Python package.
- ⁴⁵ D. Rogers and M. Hahn, *J. Chem. Inf. Mod.* **50**, 742 (2010).
- ⁴⁶ W. L. Jorgensen, J. Chandrasekhar, and J. D. Madura, *J. Chem. Phys.* **79**, 926 (1983).
- ⁴⁷ Y. Zhao and D. Truhlar, *Th. Chem. Acc.* **119**, 215 (2008).
- ⁴⁸ F. Weigend and R. Ahlrichs, *Phys. Chem. Chem. Phys.* **7**, 3297 (2005).
- ⁴⁹ M. J. Frisch, G. W. Trucks, H. B. Schlegel, G. E. Scuseria, M. A. Robb, J. R. Cheeseman, G. Scalmani, V. Barone, G. A. Petersson, H. Nakatsuji, X. Li, M. Caricato, A. V. Marenich, J. Bloino, B. G. Janesko, R. Gomperts, B. Mennucci, H. P. Hratchian, J. V. Ortiz, A. F. Izmaylov, R. Cammi, J. W. Ochterski, R. L. Martin, K. Morokuma, O. Farkas, J. B. Foresman, and D. J. Fox, “Gaussian16 Revision C.01,” (2016), gaussian Inc. Wallingford CT.
- ⁵⁰ “TURBOMOLE V7.2 2017, a development of University of Karlsruhe and Forschungszentrum Karlsruhe GmbH, 1989-2007, TURBOMOLE GmbH, since 2007; available from <http://www.turbomole.com>.”
- ⁵¹ A. D. Becke, *Phys. Rev. A* **38**, 3098 (1988).
- ⁵² R. Ahlrichs, F. Furche, and S. Grimme, *Chem. Phys. Lett.* **325**, 317 (2000).
- ⁵³ A. Schäfer, C. Huber, and R. Ahlrichs, *J. Chem. Phys.* **100**, 5829 (1994).
- ⁵⁴ F. Eckert and A. Klamt, “Cosmotherm, cosmologic gmbh&cokg, leverkusen, germany, version c2.1, revision 01.07, 2007,”.
- ⁵⁵ A. Klamt, B. Mennucci, J. Tomasi, V. Barone, C. Curchet, M. Orozco, and F. J. Luque, *Acc. Chem. Research* **42**, 489 (2009).
- ⁵⁶ A. Klamt and M. Diedenhofen, *J. Phys. Chem. A* **119**, 5439 (2015).
- ⁵⁷ S. Sinnecker, A. Rajendran, A. Klamt, M. Diedenhofen, and F. Neese, *J. Phys. Chem. A* **110**, 2235 (2006).
- ⁵⁸ R. Taft, J.-L. Abboud, M. Kamlet, and M. Abraham, *J. Solution Chem.* **14**, 153 (1985).
- ⁵⁹ T. N. Borhani, S. García-Muñoz, C. Vanesa Luciani, A. Galindo, and C. S. Adjiman, *Phys. Chem. Chem. Phys.* **21**, 13706 (2019).
- ⁶⁰ M. Bragato, G. F. von Rudorff, and O. A. von Lilienfeld, *Chem. Sci.*, (2020).